POLITECNICO MILANO
Department of Aerospace Science and Technology

FINAL ASSIGNMENT

Interplanetary & Planetary Explorer Missions

Professors: Camilla Colombo

Juan Luis Gonzalo Gomez

Group number: 05

Lyle Alexander Cambpell

Mat. 925564 ID 10683023

Giulio Pacifici

Mat. 944852 ID 10572065

Luca Rizzieri

Mat. 945691 ID 10562995

Davide Sisana

Mat. 867050 ID 10560060

Academic Year 2019/2020

Summary

Symbols

$\boldsymbol{a}$	Semi-major axis	$[km]$	$\boldsymbol{a_{pert}}$	Perturbing acceleration	$[{}^{km}/_{s^2}]$
$\boldsymbol{e}$	Eccentricity	[-]	$\boldsymbol{a_{J_2}}$	J_2 acceleration	$[{}^{km}/_{s^2}]$
$\boldsymbol{i}$	Inclination	$[deg]$	$\boldsymbol{a_{Drag}}$	Drag acceleration	$[{}^{km}/_{s^2}]$
$\boldsymbol{\Omega}$	RAAN	$[deg]$	$\boldsymbol{R_E}$	Earth mean radius	$[km]$
$\boldsymbol{\omega}$	Argument of Pericentre	$[deg]$	$\boldsymbol{R_M}$	Mars mean radius	$[km]$
$\boldsymbol{\vartheta}$	True Anomaly	$[deg]$	$\boldsymbol{\omega_E}$	Earth's angular velocity of rotation	$[{}^{rad}/_{h}]$
$\boldsymbol{TOF_H}$	Hohmann transfer time of flight	$[s]$	$\boldsymbol{M_0}$	Mean Anomaly	$[rad]$
$\boldsymbol{TOF_{par}}$	Parabolic transfer time of flight	$[s]$	$\boldsymbol{f_s}$	Sampling frequency	$[Hz]$
$\Delta\boldsymbol{v_{tot}}$	Total mission cost	$[{}^{km}/_{s}]$	$\boldsymbol{f_{cut\,off}}$	Cut-off frequency	$[Hz]$
$\Delta\boldsymbol{v_1}$	$\Delta\boldsymbol{v}$ at Neptune	$[{}^{km}/_{s}]$			
$\Delta\boldsymbol{v_2}$	$\Delta\boldsymbol{v}$ at Mars	$[{}^{km}/_{s}]$			
$\Delta\boldsymbol{v_3}$	$\Delta\boldsymbol{v}$ at Earth	$[{}^{km}/_{s}]$	**E**	Earth	
$\overrightarrow{\boldsymbol{V^-}}$	Incoming velocity in heliocentric frame	$[{}^{km}/_{s}]$	**M**	Mars	
$\overrightarrow{\boldsymbol{V^+}}$	Outgoing velocity in heliocentric frame	$[{}^{km}/_{s}]$	$\boldsymbol{N}$	Neptune	
$\boldsymbol{v_\infty}$	Excess velocity	$[{}^{km}/_{s}]$	**RAAN**	Right ascension of the ascending node	
$\boldsymbol{v_p}$	Periapsis velocity in perifocal frame	$[{}^{km}/_{s}]$	**SOI**	Sphere of Influence	
$\Delta\boldsymbol{t_f}$	Duration of flyby	$[h]$	**MJD**	Modified Julian Day	
$\boldsymbol{h_p}$	Altitude of pericenter	$[km]$	**ECI**	Earth Centred Inertial frame	
$\boldsymbol{h_{min}}$	Flyby minimum altitude	$[km]$	**GT**	Ground Track	

1. Interplanetary Explorer Mission

1.1. Introduction

The PoliMi Space Agency is conducting a feasibility study for an interplanetary mission visiting Neptune, Mars and Earth. The focus of the study is the transfer from the departure planet, Neptune, to the arrival planet, Earth, with a powered gravity assist at Mars. A preliminary mission analysis was performed to select departure, flyby and arrival dates that minimise the spacecraft powered Δv.

1.2. Design Process

1.2.1. Constraints

The mission design is carried out considering the following constraints:

- The earliest possible departure date (ED) is $1^{st}\ Jan\ 2020$;
- The latest possible arrival date (LA) is $1^{st}\ Jan\ 2060$;
- The flyby at Mars should not enter the atmosphere.

The closest gravity-assist flyby of Mars to date was performed by the *ESA mission Rosetta* in 2007 with a minimum altitude of $250\ km$[1]. Little information is available on the upper limit of Mars' atmosphere, so $250\ km$ was selected as the lower limit on flyby altitude.

1.2.2. Assumptions

The patched conics method was used, with the assumptions of zero and infinite sphere of influence (SOI) in the heliocentric and planetocentric reference frames respectively. The details of Neptune orbit departure and Earth capture were not considered. The transfers between planets were characterised by solving the Lambert problem, with instantaneous velocity vector changes at each planet. The flyby at Mars happens instantaneously with an ideal spherical gravitational field. Potential encounters with other planets and solar radiation perturbations were ignored.

1.2.3. Preliminary estimations

Maximum and minimum reference transfer times were obtained by characterising Hohmann and near-rectilinear parabolic transfers. Circular and coplanar orbits were assumed since the 3 selected planets have eccentricities smaller than $0{,}1$ and relative inclinations less than $2°$ [2]. The Hohmann transfer times were characterised analytically [3]. The cost of Hohmann transfer between Neptune and Earth was calculated for reference with `hohmannNE.m` and the value is $\Delta v = 15.71 \frac{km}{s}$.

The parabolic transfers were characterised numerically using the MatLab function `lambertMR.m` with a planetary separation angle of 10^{-4} degrees, as 0° is not compatible with the function. The planetary orbit parameters were retrieved from the function `uplanet.m` with the date selected as $1^{st}\ Jan\ 2020$. The results are provided in **Table 1**.

#	Neptune-Mars	Mars-Earth
Parabolic transfer time TOF_{par}	$13.36\ years$	$24.13\ days$
Hohmann transfer time TOF_H	$31.47\ years$	$258.87\ days$

Table 1: Reference times of flight

The synodic periods of the planet pairs were calculated to search for repetitions that could limit the size of the time windows in the optimisation. The synodic periods were estimated analytically, again assuming circular and coplanar orbits [3].

Planet	Orbital period in Earth years		Planets	Synodic Period in Earth years
Neptune	164,80		**Neptune & Mars**	1,90
Mars	1,88		**Mars & Earth**	2,13
Earth	1		**Neptune & Earth**	1,01

Table 2: Orbital and synodic periods

For the purposes of this study, the orbital motion of Neptune can be considered negligible due to its large orbital radius and low velocity. Therefore, the departure window from Neptune can be limited to 1 synodic period of Earth and Mars.

1.3. Solution methods

The Δv cost optimization problem has three dof; Neptune departure date (NDD), time of flight between Neptune and Mars (TOF_1), and time of flight between Mars and Earth (TOF_2). The optimisation aims to identify which combination of these variables produces the lowest total mission powered Δv. Two optimisation methods were used and compared: a grid search and a genetic algorithm. Both methods used the same $NDD$and TOF_1 domains. Different TOF_2 domains were used, as discussed below.

1.3.1. Grid Search

The grid is defined by the three arrays of values for NDD, TOF_1 and TOF_2 on which the search for the minimum is performed. The algorithm consists of a nested triple loop that analyses all the possible combinations of the $3\ dof$ and is summarized by the following **pseudo-code**:

```
for all values in NDD array:
 Compute Neptune position and velocity vectors at current NDD
 for all values in TOF_1 array:
  Compute Mars position and velocity vectors at current NDD + TOF_1
  Compute first Lambert arc from Neptune to Mars
  Compute Δv at Neptune
  for all values in TOF_2 array:
   if resulting arrival date is less than the LA:
    Compute Earth position and velocity vectors at NDD + TOF_1 + TOF_2
    Compute Δv at Earth
    Compute powered flyby Δv at Mars
    if constraint on h_pof hyperbola is satisfied:
     Sum the three Δvs to obtain total Δv
    end
   end
  end
 end
end
Find the minimum of total mission cost
```

The algorithm converges to the global minimum as the discretization of the grid is increased, but finer discretisation causes a significant increase of computational time. The limits of the arrays were defined using the synodic periods and reference flight times. A fine time step of 1 Earth day was used for the TOF_1 and TOF_2 arrays, while a coarse step scaled by Neptune's orbital period was used for NDD. A summary is provided in **Table 3.**

dof	Lower Boundary	Upper Boundary	Time step
NDD	ED (Earliest Departure)	$ED + T_{synME}$	165
TOF_1	TOF_{par}^{NM}	$120\%\ TOF_H^{NM}$	1
TOF_2	TOF_{par}^{ME}	$120\%\ TOF_H^{ME}$	1

Table 3: Grid search array boundaries

The grid search was implemented using the function `gridSearch.m`.

1.3.2. Genetic Algorithm

A genetic algorithm was applied to the optimization problem using the function `ga.m`. The algorithm searches for the global minimum Δv within bounded domains for each of the three variables.
Constraints must be provided for the optimisation and were specified as follows:

- $NDD + TOF_1 + TOF_2 < LA$;
- $r_p(NDD, TOF_1, TOF_2) > R_M + h_{min}$
  Where r_p is radius of Mars flyby at pericentre.

The genetic algorithm converges to the global minimum faster than a grid search over large domains. However, since the iterations of the genetic algorithm have a random nature, different runs can lead to different results. The two fundamental parameters for convergence are the population size and the maximum number of generations. The population size must be large enough to generate a wide variety of permutations. The number of generations must be high enough to reach convergence of the current run. Larger values for both parameters increase the probability that the global minimum is found, at the expense of computational time.

A good compromise between the computational time and the quality of the convergence was found with 5 runs, a population of 2000 and a maximum of generations of 300. The combination with the lowest Δv among each of the 5 runs was selected. As discussed earlier, the more important transfer is from Mars to Earth and the grid search used a restricted domain for this transfer. The global minimum may be outside this domain. The genetic algorithm was provided with a larger domain for TOF_2. $12\ years$ was selected as the maximum Mars-Earth transfer time to limit the mission length. The domains are summarised in **Table 4**.

dof	Lower Boundary	Upper Boundary
NDD	ED	$ED + T_{synME}$
TOF_1	TOF_{par}^{NM}	$120\%\ TOF_H^{NM}$
TOF_2	$24{,}13\ days$	$12\ years$

Table 4: Genetic algorithm boundaries

1.4. Results

`gridSearch.m` returns a solution with a direct transfer between Mars and Earth. The `ga.m` returns a solution with a $1\ ^{km}/_{s}$ lower mission Δv, but with a $10{,}8\ year$ transfer arc between Mars and Earth. **Figure 1** and **Figure 2** show the porkchop plots of both transfers, considering only the Δv required to depart from Neptune and to be captured at Earth. The shallow gradients in **Figure 1** and the steep gradients in **Figure 2** validate focusing the optimisation more on the Mars-Earth transfer as the total Δv is more sensitive to variation in the second transfer.

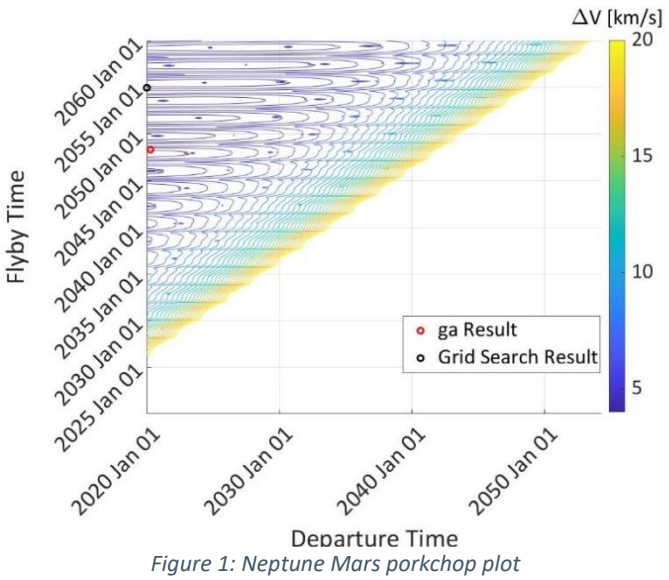

Figure 1: Neptune Mars porkchop plot

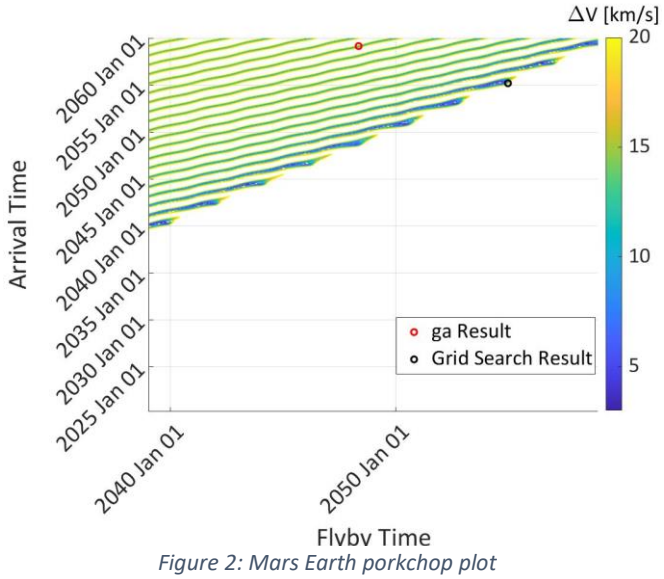

Figure 2: Mars Earth porkchop plot

Note that the solutions do not occur at optima for each leg as we are optimising for total mission Δv. In particular, the Mars-Earth leg appears to be far from optimal, but this is primarily due to the large flyby velocity at Mars making a low Δv capture at Earth impossible. The best results for each method are shown in **Table 5**.

#	$NDD[MJD]$	$TOF_1[days]$	$TOF_2\ [days]$	Normalised computational time
Grid search	7304,5000	12777,4000	85,1300	0,66
G.A.	7401,0696	10257,9821	3952,2241	1
#	$\Delta v_1\ [km/s]$	$\Delta v_2\ [km/s]$	$\Delta v_3\ [km/s]$	$\Delta v_{tot}\ [km/s]$
Grid search	4,1992	0,0714	12,5692	16,8398
G.A.	4,0979	1,7050	10,0920	15,8948

Table 5: Cost and times of the results

1.5. Final Trajectory Characterization

Since the only figure of merit for the choice of the final trajectory is the total Δv, the solution found with the `ga.m` was selected.

Departure	Flyby	Arrival
2020 *April* 06 *at* 13: 40: 10,30	2048 *May* 07 *at* 13: 14: 25,53	2059 *March* 03 *at* 18: 37: 05,26

Table 6: Dates of the final trajectory

The transfer arcs are characterized by the parameters summarized in **Table 7**.

	$a\ [km]$	$e\ [-]$	$\mathbf{i}\ [deg]$	$\Omega\ [deg]$	$\omega\ [deg]$	$\theta_i\ [deg]$	$\theta_f\ [deg]$
Neptune - Mars	$2{,}3296 \cdot 10^9$	0,9353	1,2362	45,1777	121,2306	181,5781	72,9292
Mars - Earth	$7{,}4152 \cdot 10^8$	0,8001	0,3117	343,1951	178,1618	77,9876	1,8382

Table 7: Keplerian parameters of transfer arcs

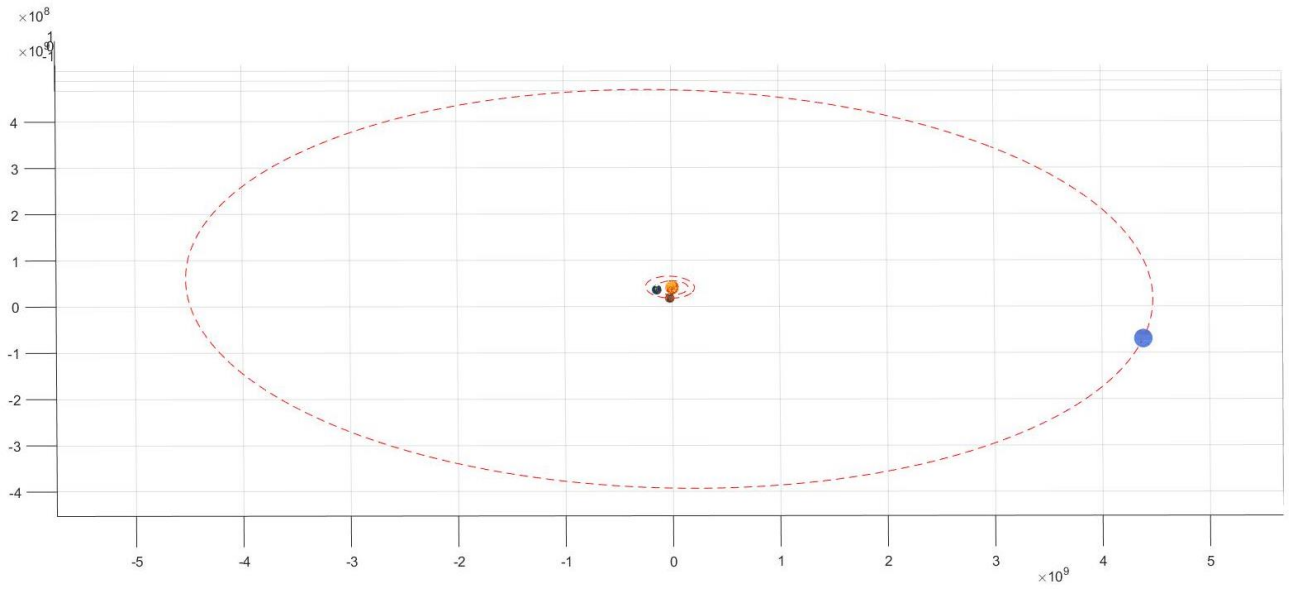

Figure 3: Departure from Neptune

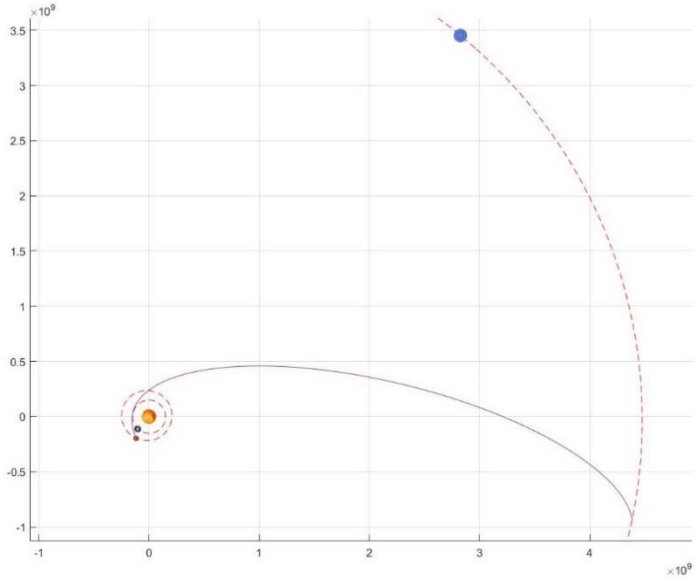

Figure 4: Neptune-Mars Transfer

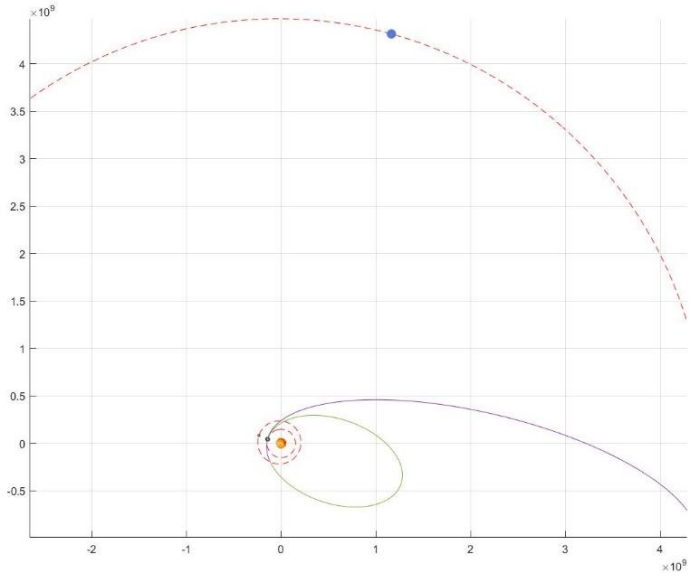

Figure 5: Mars-Earth Transfer

The heliocentric incoming and outgoing velocity vectors at Mars are:

$$\overrightarrow{V^-} = [13{,}6593 \quad -30{,}2687 \quad -0{,}6695]^T \qquad \overrightarrow{V^+} = [13{,}4802 \quad -28{,}2751 \quad -0{,}1260]^T$$

with units of km/s.

The incoming and outgoing hyperbolas of the Mars powered flyby are characterised in **Table 8**. The flyby time was calculated as the time the spacecraft was in Mars' finite sphere of influence [3].

#	h_p [km]	v_p [$^{km}/_{s}$]	v_∞ [$^{km}/_{s}$]	e [−]	TOF_f[h]
Incoming	250,0063	22,1095	21,5708	40,5449	7,4547
Outgoing	250,0063	20,4045	19,8195	34,3845	8,1125

Table 8: Flyby hyperbolas parameters

Compared to the complete mission time, $15{,}57\ hrs$ in Mars SOI is negligible and the patched conic method assumption of an instantaneous manoeuvre is valid. The total heliocentric Δv of the flyby is $\Delta v_f = 2{,}0741\ ^{km}/_{s}$ while the cost of the powered manoeuvre at the pericentre is $\Delta v_2 = 1{,}7050\ ^{km}/_{s}$. The small difference between these two indicates that the efficiency of the flyby is low and only provides a small gain compared to a deep-space manoeuvre.

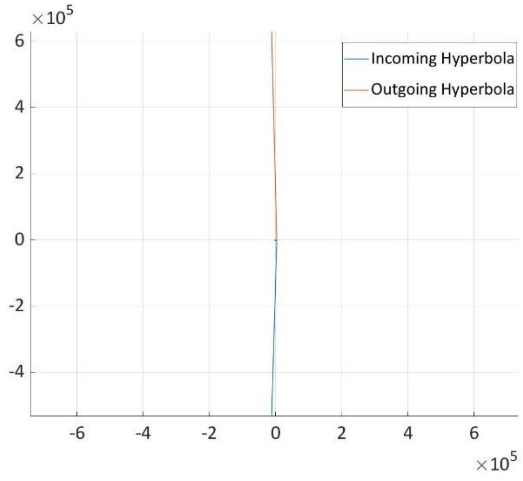

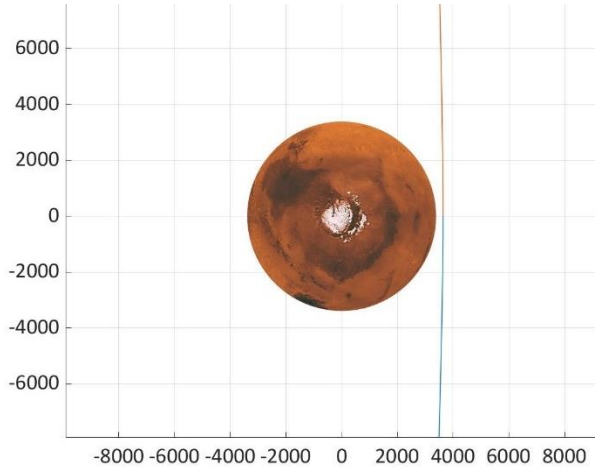

Figure 6: Mars flyby

1.6. Discussion

The solution output by the genetic algorithm was selected because the objective of the study was to minimise the powered Δv for a Neptune-Mars-Earth mission. A real mission has additional constraints requiring trade-offs. The flyby at Mars provides a relatively small gravity assist due to its small mass, as illustrated in **Table 9**, while placing a large constraint on the mission trajectory and optimisation.

Spacecraft	Flyby planet	Planet Earth mass ratio	Flyby altitude $[km]$	Δv_f $[km/s]$
Voyager	Jupiter	318	570000	16
Cassini Huygens	Venus	0,82	250	7
PoliMi	Mars	0,11	250	2

Table 9: Comparison with real missions with flybys

Additionally, the extra $10{,}8\ years$ required on the transfer orbit creates engineering and tracking costs that may not be acceptable. Unless there is a scientific reason or mission requirement to fly past Mars, it is debatable whether the flyby is justifiable as the mission Δv is practically the same as for a Hohmann transfer.

Options to reduce Δv could include flybys of large planets like Jupiter, multiple flybys of inner planets such as Earth or Venus, and aerocapture at Earth. In both trajectories discussed, approximately 70% of the mission Δv occurs at Earth. Previous sample return missions such as Stardust and Hayabusa both used Earth's atmosphere to eliminate over $12\ km/s$ of velocity [5] and this would be useful here if the mission is returning to Earth's surface.

2. Planetary Explorer Mission

2.1. Introduction

The PoliMi Space Agency plans to launch an Earth observation satellite. This study examines the proposed orbit and ground track of the spacecraft, and the effect of atmospheric drag and the J_2 perturbation. A repeating ground track is desired and a method to achieve this is presented. Two different numerical orbital propagation methods are used, and the results are compared and discussed.

2.2. Mission Data

The proposed orbit is defined by the following Keplerian elements in an Earth Centred inertial frame.

$a\ [km]$	$e\ [-]$	$i\ [deg]$	$\Omega\ [deg]$	$\omega\ [deg]$	$\theta\ [deg]$
18302	0,6158	71,5679	20	70	0

The following information on the spacecraft and its desired ground track were provided.

Earth Rotations m	Satellite Orbits k	Drag coefficient c_d	Area to mass ratio $\frac{A}{m}$
2	7	2,2	$0{,}06\ m^2/\ kg$

The spacecraft is in a prograde orbit and oscillates between Low Earth Orbit altitude when it is at the pericentre and Medium Earth Orbit altitude when it is at apocentre. It completes 7 orbits every 2 Earth sidereal days.

2.3. Perturbation Modelling

2.3.1. J_2 effect

Earth's oblate spheroid shape produces a slightly different gravitational field than that of a perfect sphere. The true gravitational field can be expressed as a series of spherical harmonics and the third term, J_2, is dominant. The perturbing acceleration is conservative and can be modelled using (§).

$$\vec{a}_{J_2} = \frac{3}{2}\frac{J_2 \mu R_E^2}{r^5}\left[\left(5\frac{z^2}{r^2}-1\right)x\,\hat{\imath} + \left(5\frac{z^2}{r^2}-1\right)y\,\hat{\jmath} + \left(5\frac{z^2}{r^2}-3\right)z\,\hat{k}\right] \qquad (§)$$

Where J_2 is a coefficient particular to the Earth, μ and R_E are the gravitational constant and radius of the Earth respectively, and x, y and z are the Cartesian coordinates of the satellite in an Earth centred reference frame.

2.3.2. Aerodynamic Drag

Aerodynamic drag significantly affects spacecraft in LEO and MEO. The acceleration due to drag is non-conservative and can be estimated using equation (§§).

$$\vec{a}_{Drag} = -\frac{1}{2}\frac{A}{m}c_D\rho(h,t)\,{v_{rel}}^2\frac{\vec{v}_{rel}}{\|\vec{v}_{rel}\|} \qquad (§§)$$

Where $\rho(h,t)$ is atmospheric density, and $\vec{v}_{rel}$ is the relative velocity between the spacecraft and the atmosphere. The time variation of atmospheric density depends on Sun interactions and is neglected for this study. The variation of atmospheric density with altitude is calculated using the exponential model of Wertz [6]. The maximum altitude considered was $1700\ km$, past which the value of density is lower than the value of the machine epsilon. $\vec{v}_{rel}$ is calculated with respect to a rotating atmosphere with a constant angular velocity equal to that of Earth.

2.4. Integration Methods

The two-body problem with non-conservative perturbations can be solved by numerical integration in Cartesian coordinates, or with respect to the Keplerian elements by using the Gauss Planetary Equations (GPE)[3]. Both methods in `orbitintegration.m` report the Cartesian and Keplerian states of the spacecraft at each time step using `car2par.m` (for cartesian to Keplerian) and `car2par.m` (for Keplerian to cartesian). Integration is performed with MATLAB solver `ode113` with a relative tolerance of $10^{-13}$and absolute tolerance of 10^{-14}.

2.4.1. Integration in Cartesian Coordinates

The initial Cartesian position and velocity are found from the initial Keplerian elements. The components of the perturbing accelerations are evaluated for each direction and the Cartesian state vector's derivatives are calculated as follows:

$$\frac{d}{dt}\begin{Bmatrix}\vec{r}\\ \vec{v}\end{Bmatrix} = \begin{Bmatrix}\vec{v}\\ -\frac{\mu}{r^3}\vec{r} + \vec{a}_{pert}\end{Bmatrix}$$

Where: $\vec{a}_{pert} = \vec{a}_{J_2} + \vec{a}_{Drag}$, $\vec{r}$ is the spacecraft position, and $\vec{v}$ is the spacecraft velocity
The orbit propagation in Cartesian coordinates is implemented in the function `odeCart.m`.

2.4.2. Integration of Gauss Planetary Equations

In the GPE method the variation of the Keplerian elements is solved for each time step. The Cartesian components of the perturbing accelerations are evaluated and then converted to tangential $\hat{t}$, normal $\hat{n}$ and out of plane $\hat{h}$ components for the GPE method.

$$\frac{d}{dt}\vec{K} = f\left(\vec{K}, \vec{a}_{pert}{}^{(tnh)}\right)$$

Where: $\vec{K} = [a \quad e \quad i \quad \Omega \quad \omega \quad \theta]^T$ and $\vec{a}_{pert}{}^{(tnh)} = \left[\hat{t} \mid \hat{n} \mid \hat{h}\right]^T \vec{a}_{pert}{}^{(cart)}$

2.5. Ground Tracks

A stable orbit around a spherical body would trace an identical ground track every orbit. The real ground tracks of spacecraft orbiting Earth are affected primarily by the Earth's rotation and by the J_2 perturbation. The Earth rotates eastward at $15{,}04°$ per hour, causing a generic ground track to drift westward. J_2 effects cause periodic oscillation of the Keplerian elements and long term, secular evolution of the $RAAN$, argument of perigee and mean anomaly [3]. The rate of the secular evolutions can be with the equations in **Table 10** and the rates are shown for the provided orbit. In order for the ground track to repeat, equation (§§§) should hold for the unperturbed case and equation (§§§§) should hold when the effects of J_2 are included. Some orbit properties as well as the secular J_2 effects for the provided orbit are calculated in **Table 10**.

$$k \cdot T \cdot \omega_E = m \cdot 2\pi \qquad (§§§)$$

$$\frac{m}{k} = \frac{\omega_E - \dot{\Omega}}{n + \dot{M}_0 + \dot{\omega}} \qquad (§§§§)$$

	$\dot{\Omega}$	$\dot{\omega}$	$\dot{M}_0$
Secular evolution $[deg/s]$	$-2{,}3587 \cdot 10^{-6}$	$-1{,}8656 \cdot 10^{-6}$	$2{,}6114 \cdot 10^{-6}$

Table 10: Secular evolutions caused by the J_2effect

The true satellite ground track can be estimated by propagating the orbit and projecting the satellite's position onto the Earth's surface. This projection maps to the latitudes and longitudes where the satellite passes through the local zenith. The satellite ground track is calculated with the function `GT.m`.

2.5.1. Non-repeating Ground Track

The satellite ground track was evaluated for the provided orbit over three different time periods: 1 orbital period, 1 day and 10 days. For each case the integration was performed for both the unperturbed and J_2 perturbed cases. All cases included the rotation of the Earth.

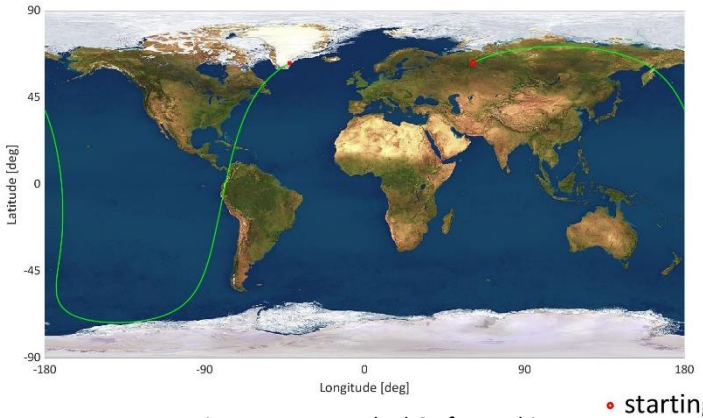

Figure 7: Unperturbed GT for 1 orbit

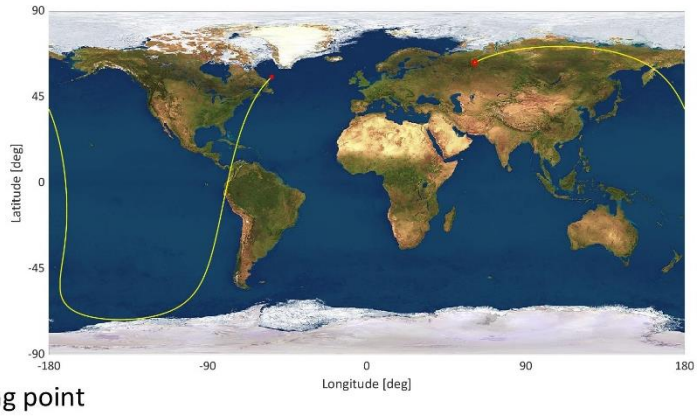

Figure 8: Perturbed GT for 1 orbit

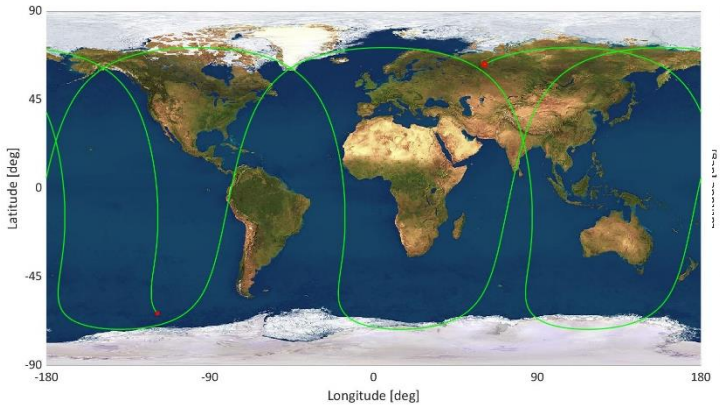

Figure 9: Unperturbed GT for 1 day

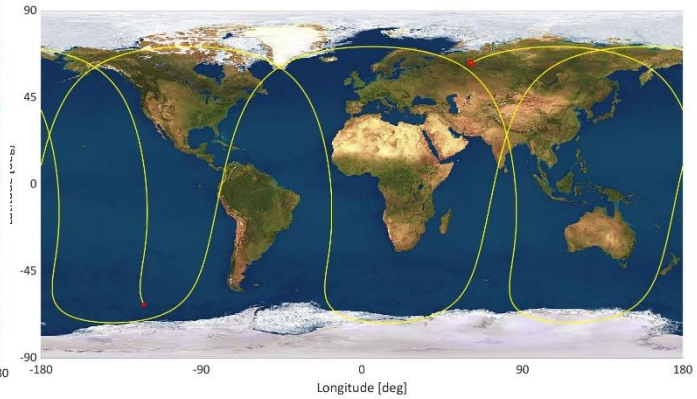

Figure 10: Perturbed GT for 1 day

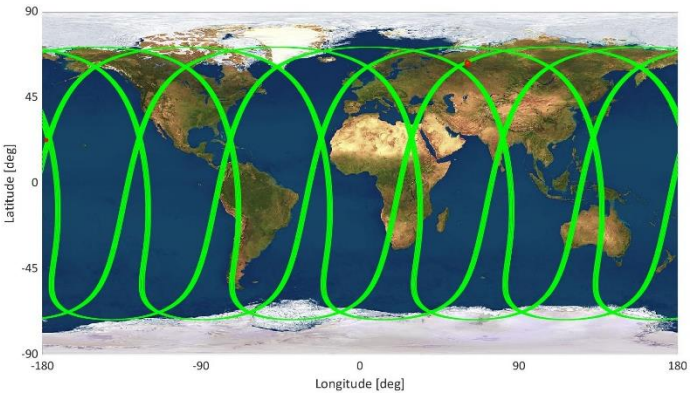

Figure 11: Unperturbed GT for 10 day

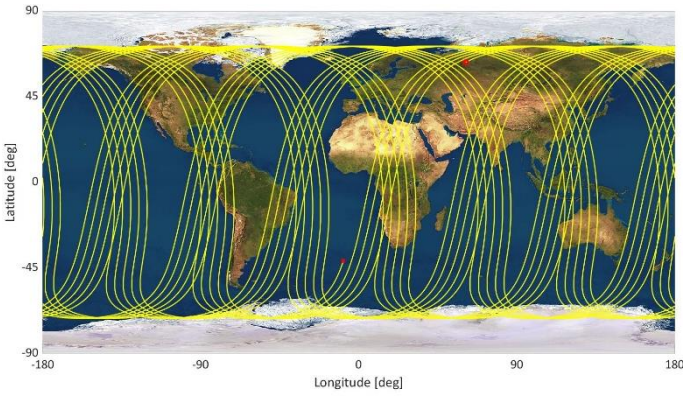

Figure 12: Perturbed GT for 10 day

As expected, there is a slight westward drift in the unperturbed ground track. When the J_2 effect is introduced, a larger westward drift occurs. This is also expected as the J_2 effect causes westward drift in prograde orbits [3].

2.5.2. Repeating Ground Track

The mission requirements specify that the ground track should repeat every m Earth rotations and k satellite orbits. Modified orbital parameters are necessary to meet this requirement for both J_2 perturbed and non-perturbed cases. For an orbit with constant inclination and eccentricity, the variables in equation (§§§§) are a function of a only. The equation can be solved numerically for the value of a for a given ratio m/k. This is implemented in the function `repGTJ2.m`, for both the perturbed and unperturbed cases and the results reported in **Table 11**.

#	Original Orbit	Unperturbed orbit	J_2 perturbed orbit
$a\ [km]$	18302	18284,4713	18290,7518

Table 11: Variations of semi major axis

It can be noticed that the perturbed ground track does not precisely repeat due to short term, non-secular oscillations in the orbital elements, caused by J_2.

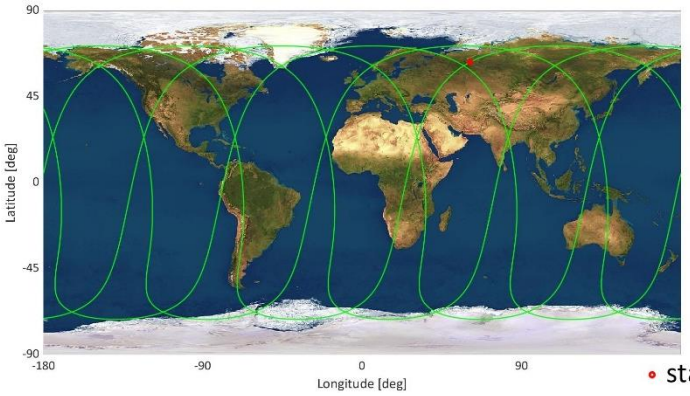

Figure 13: Unperturbed repeating GT

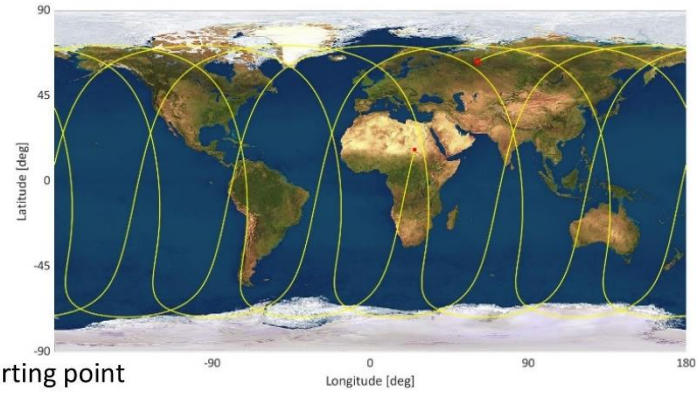

Figure 14: Perturbed repeating GT

2.6. Orbit Propagation

2.6.1. Integration Method Comparison

For evaluating the accuracy, the infinity norm error was evaluated between the final Keplerian elements of the Cartesian and GPE schemes and the relative difference reported in **Table 12**. The propagations covered 100 orbits with time steps of $500\ seconds$. This corresponds to approximately $28{,}5\ days$ with 49 steps per orbit. The final infinity norm for the semi-major axis was $0{,}2\ m$. The magnitude of this difference is such that the two solutions can be considered equivalent.

$a\ [km]$	$e\ [-]$	$i\ [deg]$	$\Omega\ [deg]$	$\omega\ [deg]$	$\theta\ [deg]$
$2{,}0019 \cdot 10^{-4}$	$4{,}2074 \cdot 10^{-9}$	$2{,}2819 \cdot 10^{-8}$	$4{,}7728 \cdot 10^{-8}$	$3{,}0187 \cdot 10^{-7}$	$9{,}4882 \cdot 10^{-5}$

Table 12: Infinity norm errors of Keplerian elements between GPE and Cartesian methods

To compare computation efficiency, $100\ orbits$ were integrated, with a range of time step increments, using both $Cartesian$ and GPE methods. The results are shown in **Figure 15**. The faster solution time of the GPE method is likely due to the lower magnitude of the derivatives in the Keplerian state vector, requiring few iterations in the numerical ODE solver. The GPE method was used to obtain all following results.

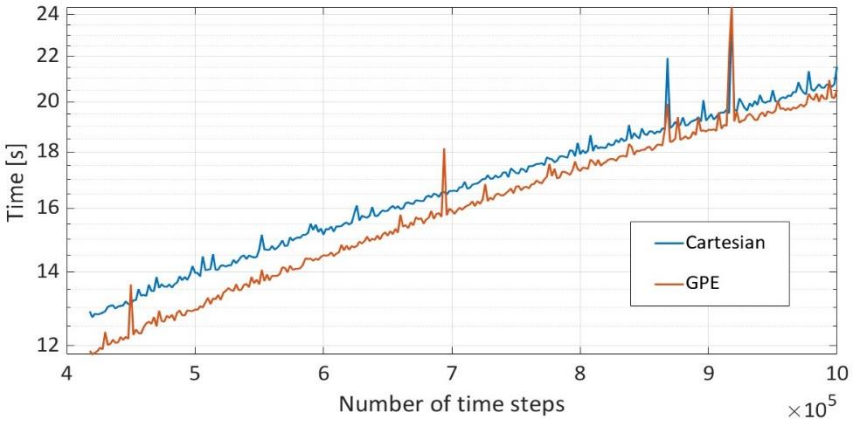

Figure 15: Comparison in computational time

2.6.2. Time Evolution of Keplerian Elements

The spacecraft orbit was propagated for $10\ years$ using the GPE method to observe the long-term effects of the J_2 perturbation and drag, and the results are plotted in **Figure 16**. The time step used was $500\ seconds$.

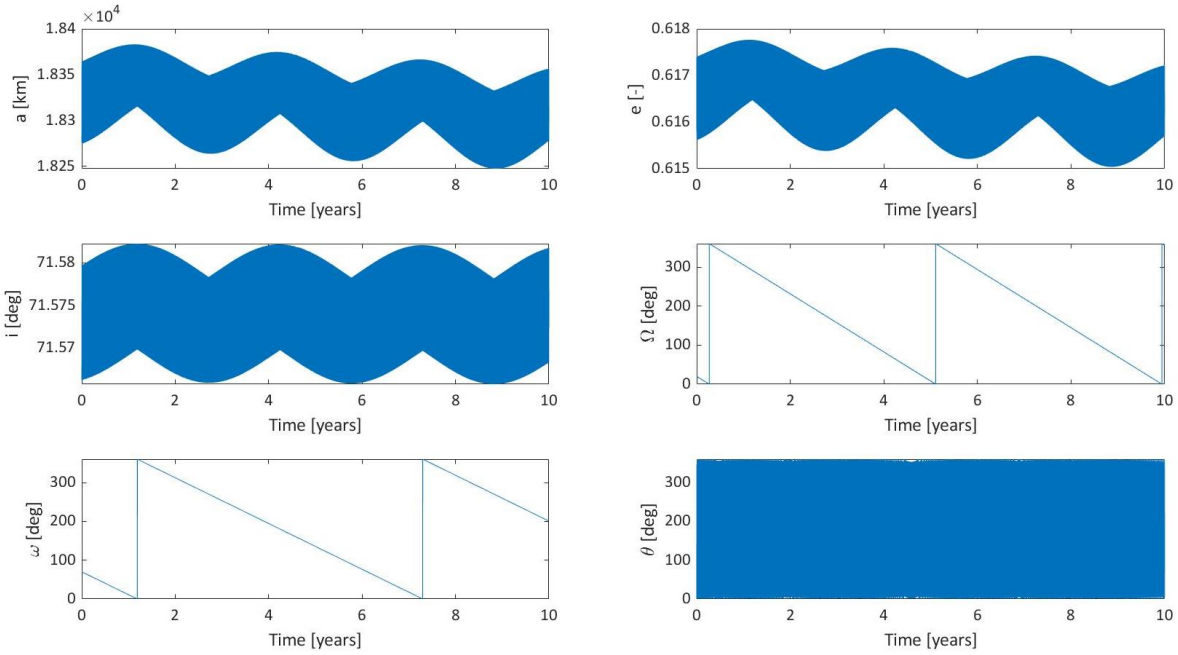

Figure 16: Keplerian elements evolution over 10 years

The following trends are clear from **Figure 16:**

- a and e have a secular decay due to aerodynamic drag.
- a, e and i have long term oscillations with a period of about 3 years due to J_2 effects.
- Ω and ω have a secular regression due to J_2 effects.
- All elements have relatively large short-term oscillations.

2.6.3. Time Evolution of Orbit

The time evolution of the orbit is represented in **Figure 17**. The orbit is propagated for 1 year with one orbit plotted every week. A dotted apse line is also shown.

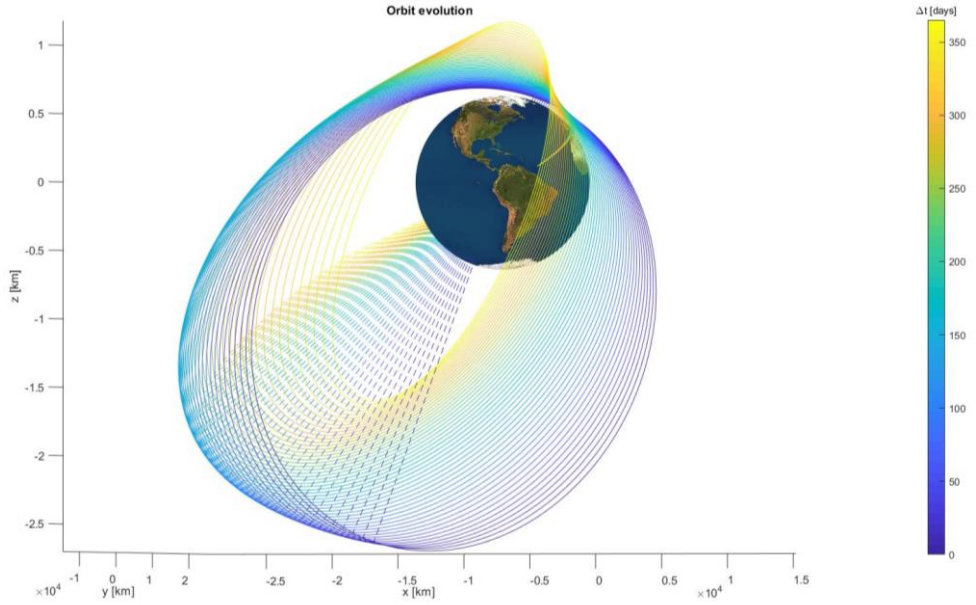

Figure 17: Orbit evolution over 1 year

2.6.4. Frequency Analysis

The frequency characteristics of the orbital elements were analysed to identify the dominant perturbation frequencies and relative magnitudes. True anomaly was excluded from the analysis. The function `fft.m` is used to calculate the Fourier transform of each orbital element with the settings in **Table 13**.

Sampling range	Sampling Period	Number of samples	Sampling frequency	Resolution frequency
$10\ years$	$500\ seconds$	630720	$2 \cdot 10^{-3} Hz$	$3{,}17 \cdot 10^{9}$

Table 13: Samplings parameters

Figure 18 shows the single sided spectra of the Fourier transform for each element, in absolute values. The values for the frequency of $0\ Hz$ are not plotted in order to better visualize the orbit perturbation frequencies. Note that the orbital period is $6{,}8447\ hours$, corresponding to a frequency of $0{,}4058 \cdot 10^{-4} Hz$.

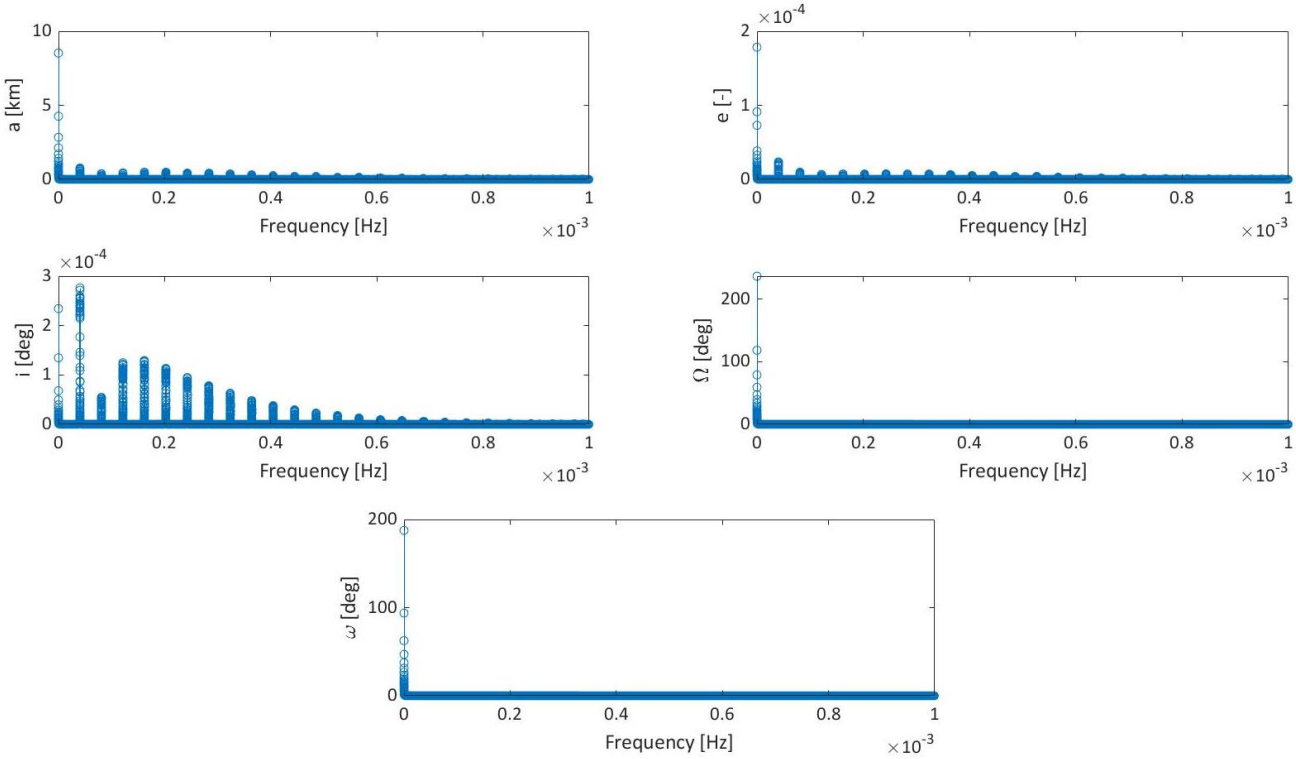

Figure 18: Fourier analysis of keplerian elements

The following observations can be made:

- a and e have a large, near-secular variation due to drag, indicated by the peak near $0\ Hz$.
- a, e and i have short- and long-term variations with frequencies that are integer multiples of orbital frequency due to J_2 effect.
- Ω and ω frequency response are dominated by secular J_2 effects.

Filtering of the evolution of the Keplerian elements was performed using both a time domain filter and a frequency domain filter. The time domain filtering is performed with a centered moving average function, which replaces each entry with the local average over a small window, where the window is centered on the current entry. The function `movmean.m` was used. The selected cut off frequencies for the frequency domain filter are reported in **Table 14**.

a	e	i	Ω	ω
$10^{-8}\ Hz$	$10^{-8}\ Hz$	$10^{-8}\ Hz$	$6 \cdot 10^{-8}\ Hz$	$6 \cdot 10^{-8}\ Hz$

Table 14: Cut-off frequencies for each Keplerian element

The number of samples that belong to the window for each Keplerian element is calculated as follows:

$$k_{el} = \frac{f_s}{2} \cdot \frac{1}{f_{cutoff_{el}}}$$

The frequency domain filter sets the magnitude to zero of the points outside the cut-off frequency. The filtered time evolution of the element is then retrieved by performing the inverse Fourier transform of the filtered spectrum using the function `ifft.m`. The selected cut off frequencies for the frequency domain filter are reported in **Table 15**.

a	e	i	Ω	ω
$10^{-6}\ Hz$	$10^{-6}\ Hz$	$10^{-6}\ Hz$	$4 \cdot 10^{-6}\ Hz$	$4 \cdot 10^{-6}\ Hz$

Table 15: Cut-off frequencies for each Keplerian element

The selected cut off frequencies are lower for the time domain filter due to its reduced high-frequency attenuation compared to the frequency domain filter. The original evolution and both filtered evolutions of the Keplerian elements are shown in **Figure 19**.

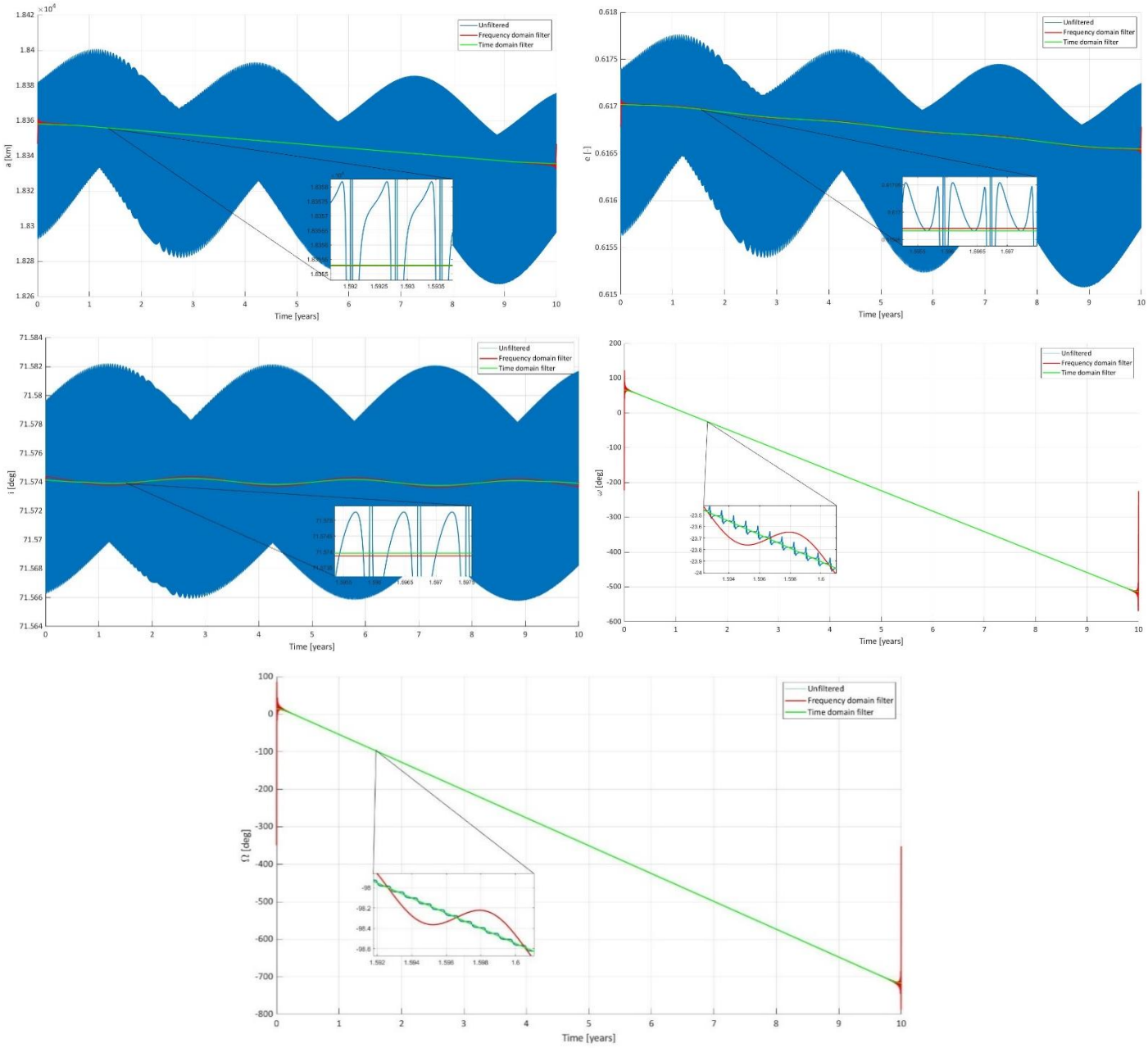

Figure 19: Unfiltered e filtered evolution of Keplerian

Both filters have large relative errors at the boundaries of the observation window. The time-domain filter errors occur as the moving average is calculated over a reduced sample size at the boundaries. The frequency domain filter errors are a property of the inverse Fourier transform with a finite data set.

2.7. Real Data Comparison

Results from the $NASA\ JPL\ HORIZONS$ [7] ephemeris generator with orbital data from a real satellite were used as a comparison for the results calculated in this report. An inactive satellite was selected as it will not be performing station keeping maneuvers and its elements will evolve naturally.
The $satellite\ KIKU\text{-}3(ETS\text{-}IV)$ was selected. It is an engineering test satellite launched by JAXA in 1981 that was deactivated in 1984 [8] The orientation and stability of the satellite are not known, so the cylindrical diameter and mass listed on the satellite data sheet were used to estimate a circular area to mass ratio and tumbling was neglected. The drag coefficient was not changed from the initial value of $c_d = 2{,}2$.

Perigee altitude	Apogee altitude	Inclination	Diameter	Mass	A/m	c_d
$225\ km$	$36000\ km$	28,5°	$2{,}1\ m$	$638\ kg$	0,0054	2,2

Table 16: Satellite KIKU-3 parameters

The satellite orbit was propagated from $1^{st}\ January\ 1985$ to $1^{st}\ January\ 1986$ in both the $NASA\ JPL\ HORIZONS$ and MatLab models. In **Figure 20**, the time evolution of Keplerian elements is compared. For reference, the MatLab model was also run with the provided A/m ratio of the planetary explorer spacecraft.

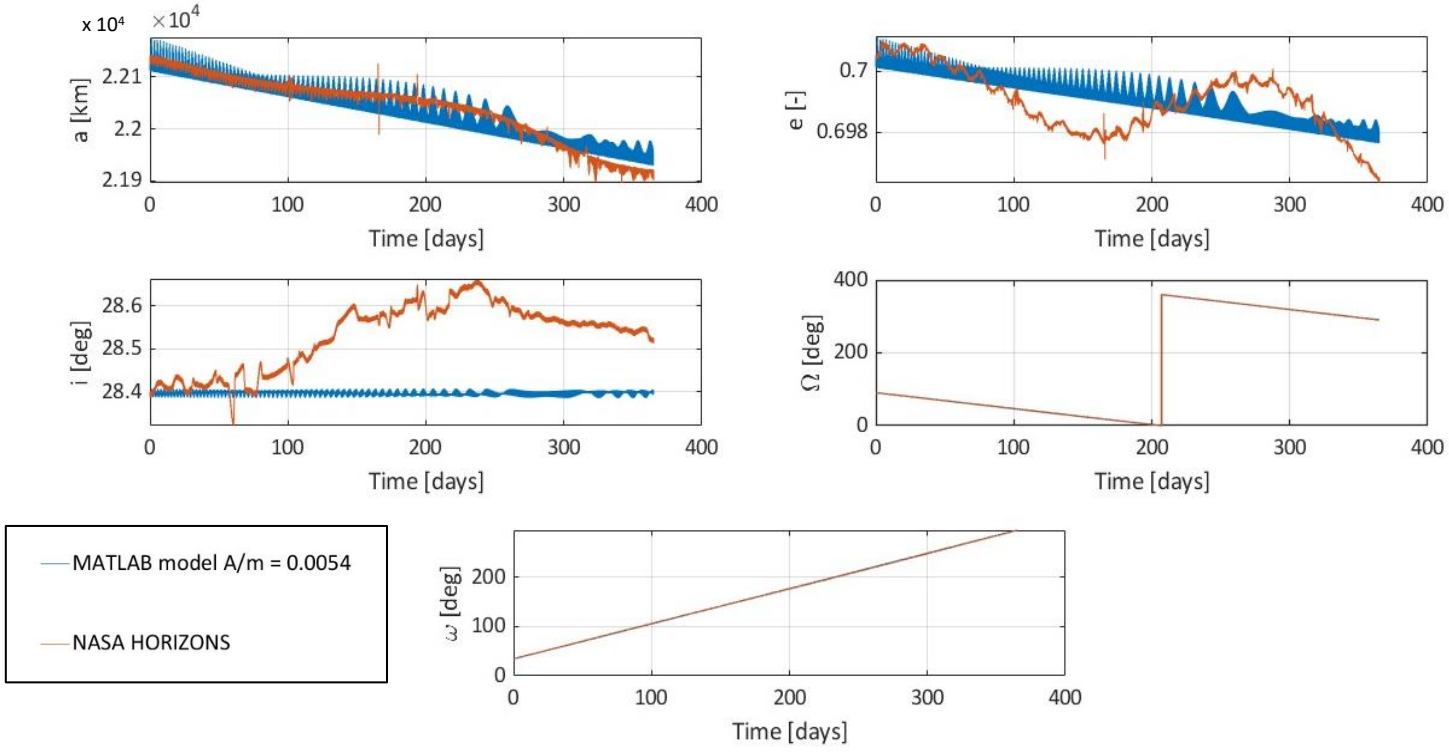

Figure 20: Comparison between real data and MatLab integration

The evolution of the a and the eccentricity of $KIKU\text{-}3$ are well estimated by the MatLab model. A $1\ year$period oscillation occurs in the $NASA\ JPL\ HORIZONS$ model, possibly due to solar radiation pressure [3].

The secular evolution of Ω and ω are also well estimated, with only a small difference from the $NASA\ JPL\ HORIZONS$ model. Almost zero long-term inclination change is predicted by the MatLab model as drag and J_2 have negligible long-term effects on inclination. The differences compared to the $NASA\ JPL\ HORIZONS$ model are likely due to $SRP$and Moon perturbations.

3. References

[1] ESA, *Rosetta Flyby of Mars,* September 2019, <https://sci.esa.int/web/rosetta/-/28611-rosetta-flyby-of-mars>.

[2] NASA, *Planetary Fact Sheet – Metric,* October 2019, <https://nssdc.gsfc.nasa.gov/planetary/factsheet/>.

[3] Curtis, H.D., *Orbital Mechanics for Engineering Students*, 2005, Elsevier Butterworth-Heinemann, MA, USA.

[4] NASA, Trajectories - Voyager 2 Gravity Assist Velocity Changes, <https://solarsystem.nasa.gov/basics/chapter4-1/>

[5] Cassel et. al, Hayabusa Re-entry Trajectory Analysis and Mission Design, 2012, NASA Ames Reseach Centre,

[6] Wertz, 1978, 820.

[7] NASA/JPL's HORIZONS, <https://ssd.jpl.nasa.gov/hotizons.cgi.>.

[8] JAXA, *Engineering Test Satellite IV "KIKU-3",*<https://global.jaxa.jp/projects/sat/ets4/index.html>.